Hyperbolic normal stochastic volatility model

Jaehyuk Choi
Peking University HSBC Business School, Shenzhen, China, jaehyuk@phbs.pku.edu.cn
Chenru Liu
Peking University HSBC Business School, Shenzhen, China, 1501213463@sz.pku.edu.cn
Byoung Ki Seo
Ulsan National Institute of Science and Technology, Ulsan, Korea, bkseo@unist.ac.kr

For alternative options pricing models and heavy-tailed distributions, this study proposes and analyzes a continuous-time stochastic volatility (SV) model based on an arithmetic Brownian motion. The normal stochastic alpha-beta-rho model is a special case of our model. Using the generalizations from Bougerol's identity in the literature, we propose a closed-form simulation scheme, efficient quadrature integration for vanilla options pricing, and fast moment-matching method. Furthermore, the transition probability of another special case is given by Johnson's S_U curve, a popular heavy-tailed distribution with superior analytical tractability. Therefore, our model serves as an analytically tractable SV model and heavy-tailed distribution backed by stochastic differential equations.

Key words: stochastic volatility, SABR model, Bougerol's identity, Johnson's S_U distribution

1. Introduction

Stochastic volatility (SV) models have been proposed to overcome the failure of the Black-Scholes-Merton (BSM) model in explaining non-constant implied volatilities across strike prices on option markets, a phenomenon called volatility smile. Therefore, most previous studies (e.g., Hull and White (1987), Stein and Stein (1991), Heston (1993)) focus on SV models based on geometric Brownian motion (BM) (thereafter, lognormal SV models). On the other hand, SV model studies based on arithmetic BM (thereafter, normal SV models) are scarce. This study aims to fill this gap by proposing and analyzing a class of normal SV models. Our motivation for choosing arithmetic BM as the *backbone* of the SV model are twofold: an options pricing model alternative to the lognormal SV model and a skewed and heavy-tailed distribution family generalizing the normal distribution.

We first discuss the options pricing model. Although eclipsed by the success of the BSM model, the arithmetic BM was analyzed for the first time as an options pricing model by Bachelier (1900) (thereafter, normal model) and still provides more relevant dynamics than the geometric BM for some financial asset classes. See Brooks and Brooks (2017) and Schachermayer and Teichmann (2008) for recent surveys on the normal model. Interest rate is a first example. The proportionality

between the daily changes and level of interest rate, a key assumption of the BSM model, is empirically weak (Levin 2004). Therefore, among fixed-income market traders, the normal model has long been a popular alternative to the BSM one for quoting and risk-managing the options on interest rate swap and Treasury bonds (and futures). An important difference between them is that the volatility under the arithmetic BM (thereafter, normal volatility), which measures the uncertainty for an absolute, not relative, change of interest rate. For example, Merrill Lynch option volatility index (MOVE), the equivalent of the VIX index for the fixed-income market, is calculated as the weighted average of the normal implied volatilities of the US Treasury bond yield. It is also worth noting that the hedging ratio, delta, from the normal and BSM models can be often significantly different, although the volatilities of the corresponding models are calibrated to the same option price observed on the market. Therefore, the normal model's delta provides more efficient hedging if market conditions are similar to the assumptions of the normal model. The use of the normal model for the interest market is further justified by the negative policy rates observed in several developed economies after the global financial crisis of 2008. Other than the interest rate, the normal model is often used for modeling the inflation rate (Kenyon 2008) and spread option (Poitras 1998).

Despite this background, studies on the normal SV model are rare. The scarcity of the normal SV model is even more surprising considering lognormal SV models are often analyzed under the framework of normal diffusion on the log price variable, meaning the solution methods for the lognormal SV models can be applied to the corresponding normal SV model with minimal modifications. To the best of our knowledge, the only previous study on the normal SV model is in the context of the stochastic alpha-beta-rho (SABR) model (Hagan et al. 2002), an SV model popular among practitioners. In SABR, the price follows a constant elasticity of variance (CEV) backbone, while the volatility follows a geometric BM. Therefore, the model provides a range of backbone choices, with normal and lognormal backbones being the two extremes. The normal SV model we propose is inspired by (i.e., is a special case of) the SABR model with normal backbone. For a more in-depth review of the SABR model, see § 2.2.

We propose and analyze a class of normal SV models, which includes the normal SABR model as a special case. Since it is closely related to the BMs in hyperbolic geometry (and involves hyperbolic functions), we name the class *hyperbolic normal SV* model or NSVh model, as an abbreviation similar to how hyperbolic sine becomes sinh. Based on the generalized Bougerol's identity (Alili et al. 1997, Alili and Gruet 1997), we equip the NSVh model with two tools critical to the success of any SV model: (i) an exact closed-form simulation method and (ii) vanilla options pricing with efficient quadratures integration. Notably, our simulation scheme requires merely one and a half (1.5) normal random numbers for a transition between time intervals of any length. The vanilla

option price is more efficient than previous integration representations (Henry-Labordère 2008, Korn and Tang 2013, Antonov et al. 2015), in that our expression can be accurately evaluated with numerical quadratures. Additionally, we provide a simpler proof of the key mathematical result of Alili and Gruet (1997).

The second aspect of our study is that the distributions resulting from the normal SV models can incorporates skewness and heavy-tail generalizing of the normal distribution. Heavy-tailed distributions occur everywhere, and their importance cannot be emphasized enough. In this regard, the study of normal SV models has a much broader significance than that of lognormal SV models, since the latter generalize the lognormal distribution, whose application is rather limited compared to the normal distribution.

A large number of distribution families has been suggested by the statistics community to incorporate skewness and heavy tails into a normal distribution. Even if we narrow our focus to finance literature, the following are examples of the distributions to model asset returns: generalized lambda (Corlu and Corlu 2015), stable (Fama 1965), skewed t (Theodossiou 1998), Gaussian mixture (Kon 1984, Behr and Pötter 2009), generalized hyperbolic (Eberlein et al. 1995, Behr and Pötter 2009), Turkey's g- and h- (Badrinath and Chatterjee 1988, Mills 1995), and Johnson's S_U (thereafter S_U) distribution (Shang and Tadikamalla 2004, Gurrola 2007, Choi and Nam 2008).

Most such distributions are obtained from the generalizations of the normal probability density function (PDF) or the transformations of the normal random variable. To the best of our knowledge, no heavy-tailed distribution is either defined from or associated with a continuous-time stochastic process, including the SV model. This is because, in general, it is difficult for a stochastic differential equation (SDE) to yield an analytically tractable solution. There are only a few examples of continuous-time diffusion models whose transition probabilities are associated with well-known distributions: arithmetic BM with normal distribution (by definition), geometric BM with lognormal distribution, and CEV and CIR processes with non-central χ^2 distribution.

Our study adds to the literature by showing that the transition probability for a special case of the NSVh model (different from the normal SABR case) is given by the S_U distribution (Johnson 1949). The S_U curve has become increasingly popular for modeling heavy-tailed distributions in numerous fields due to its computational flexibility (see § 2.3 for a review of S_U). Our finding that the S_U distribution comes from an SV model provides the theoretical justification for the popularity of S_U. The NSVh model provides a more intuitive representation of S_U and generalizes the S_U distribution.

Overall, an important contribution of the NSVh model is that it bridges two unrelated topics: SV models from financial economics and heavy-tailed distributions from statistics. There are many

benefits from the interchangeable usage of the two. For example, the S_U distribution is now recognized an options pricing model with superior analytic tractability: vanilla option price, density functions, skewness, ex-kurtosis, value-at-risk (VaR), and expected shortfall (ES) have closed-form expressions that are not available in the normal SABR model. Moreover, we show that the two distributions are very similar if calibrated to the same option prices or moments through empirical examples, thus can be used interchangeably. We propose a rapid method to find equivalent parameter sets based on moment matching.

This remainder of this paper is organized as follows. Section 2 defines the NSVh model and reviews the SABR model and the S_U distribution. Section 3 describes the main results. Section 4 presents the numerical results with empirical data. Finally, Section 5 concludes the paper.

2. Models and Preliminaries

2.1. NSVh Model

We introduce the NSVh model as

$$dF_t = \sigma_t \left(\rho \, dZ_t^{[\lambda\alpha/2]} + \rho_* \, dX_t \right) \quad \text{and} \quad \frac{d\sigma_t}{\sigma_t} = \alpha \, dZ_t^{[\lambda\alpha/2]}, \tag{1}$$

where F_t and σ_t are the processes for the price and volatility, respectively, α is the volatility of the volatility parameter, and ρ the instantaneous correlation between F_t and σ_t with the orthogonal component, $\rho_* = \sqrt{1-\rho^2}$. In our setting, Z_t and X_t are independent BMs and $Z_t^{[\mu]} = Z_t + \mu\, t$ denotes BM with drift μ. Similar to lognormal SV models, correlation ρ accounts for the asymmetry in the distribution (e.g., skewness or slope of the volatility smile) and α for the heavy tail (e.g., excess kurtosis or convexity of the volatility smile). The so-called leverage effect, the negative correlation between spot prices and volatility, is explained with a negative ρ, although it is in the context of normal volatility.

Note that drift $\lambda\alpha/2$ is applied to Z_t in both SDEs for F_t and σ_t in the NSVh model. Drift parameter λ plays a role of constant elasticity for σ_t in that $(\sigma_t)^{1-\lambda}$ is a martingale:

$$\begin{aligned} \frac{d(\sigma_t)^{1-\lambda}}{(\sigma_t)^{1-\lambda}} &= (1-\lambda)\alpha \, dZ_t \quad \text{if} \quad \lambda \neq 1, \\ d(\log \sigma_t) &= \alpha \, dZ_t \quad \text{if} \quad \lambda = 1. \end{aligned}$$

For example, $\lambda = 0$ yields the volatility process of the SABR model and $\lambda = -1$ that of Hull and White (1987).

However, note that F_t is martingale only when $\lambda = 0$ (or, less importantly, $\rho = 0$), owing to the drift. The NSVh model with $\lambda = 0$ is the SABR model with normal backbone which is subsequently introduced, and has been an important motivation for this study. Although it may not be a desirable price process, the NSVh model for $\lambda \neq 0$ may be understood as the probability distribution

perturbed from base case $\lambda = 0$, according to the Girsanov theorem. As subsequently discussed, λ does not significantly increase the structural diversity of the distribution, hence a *perturbation* rather than a *generalization*. Nevertheless, the introduction of λ sheds light on the general understanding of the NSVh model: λ connects the normal SABR ($\lambda = 0$) to Johnson's S_U distribution ($\lambda = 1$).

While volatility σ_t is analytically integrated to

$$\sigma_t = \sigma_0 \exp\left(\alpha Z_t^{[\frac{1}{2}(\lambda-1)\alpha]}\right), \tag{2}$$

price F_t is integrated as below for a fixed time T:

$$F_T - F_0 = \frac{\rho}{\alpha}\big(\sigma_T - \sigma_0\big) + \rho_* \int_0^T \sigma_t dX_t.$$

As F_t is not a martingale in general, it is better to rewrite the integral using the expectation of F_T, $\bar{F}_T = F_0 + (\sigma_0\rho/\alpha)\big(e^{\frac{1}{2}\lambda\alpha^2 T} - 1\big)$:

$$F_T - \bar{F}_T = \frac{\rho}{\alpha}\big(\sigma_T - \sigma_0\, e^{\frac{1}{2}\lambda\alpha^2 T}\big) + \rho_* \int_0^T \sigma_t dX_t. \tag{3}$$

We now simplify the expressions into canonical forms by the following changes of variables:

$$s = \alpha^2 t\ (S = \alpha^2 T), \quad \tilde{\sigma}_s = \frac{\sigma_t}{\sigma_0}, \quad \text{and} \quad \tilde{F}_s = \frac{\alpha}{\sigma_0}\big(F_t - \bar{F}_T\big),$$

where the new time variable s is the integrated variance of log volatility. Therefore, the NSVh distribution is effectively parametrized by five parameters, ($\bar{F}_T$, σ_0/α, $\alpha^2 T$, ρ, λ). The SDEs and joint distributions at $s = S$ are respectively cast into the following canonical forms:

$$d\tilde{F}_s = \tilde{\sigma}_s(\rho\, dZ_s^{[\lambda/2]} + \rho_*\, dX_s) \quad \text{and} \quad d\tilde{\sigma}_s = \tilde{\sigma}_s\, dZ_s^{[\lambda/2]} \quad (\tilde{\sigma}_0 = 1), \tag{4}$$

$$\tilde{F}_S \overset{d}{=} \rho\left(e^{Z_S^{[\frac{1}{2}(\lambda-1)]}} - e^{\frac{1}{2}\lambda S}\right) + \rho_*\, X_{A_S^{[\frac{1}{2}(\lambda-1)]}} \quad \text{and} \quad \tilde{\sigma}_S = \exp\left(Z_S^{[\frac{1}{2}(\lambda-1)]}\right), \tag{5}$$

where $\overset{d}{=}$ denotes the equality in the distribution law. Here, the integral term of (3), the part of price transition uncorrelated to volatility, is further simplified with the exponential functional of BM defined by

$$A_T^{[\mu]} = \int_{t=0}^T e^{2Z_t^{[\mu]}} dt, \tag{6}$$

which has been the topic of extensive research (Matsumoto and Yor 2005a,b, Yor 2012). While inspired from the time-integrated price under the BSM model in the context of continuously monitored Asian options, the exponential functional, $A_S^{[\frac{1}{2}(\lambda-1)]}$ in this study denotes time-integrated variance. Although the functional $A_T^{[\mu]}$ can be defined with *any* standard BM, throughout this paper, we implicitly assume $A_T^{[\mu]}$ is tied to specific BM Z_t, driving volatility process. This is because the conditional distribution of $A_T^{[\mu]}$ on Z_T is a quantity of interest. While we distinguish between the original and canonical forms in the rest of this paper, we often use $S\,(= \alpha^2 T)$ in the original form for the sake of concise notation.

2.2. SABR Model and BM on Hyperbolic Geometry

Here, we review the SABR model with a focus on the normal case. Our approach is also compared to those of the previous studies. The SABR model (Hagan et al. 2002) is an SV model with a CEV backbone:

$$\frac{dF_t}{F_t^\beta} = \sigma_t \left(\rho dZ_t + \rho_* dX_t\right) \quad \text{and} \quad \frac{d\sigma_t}{\sigma_t} = \alpha\, dZ_t \quad \text{for} \quad 0 \le \beta \le 1, \tag{7}$$

where X_t and Z_t are independent BMs. Therefore, the SABR model with $\beta = 0$ (thereafter normal SABR) is equivalent to the NSVh model with $\lambda = 0$. The effects of parameters ρ and α are similar to those in the NSVh model.

The SABR model has been widely used in the financial industry due to several merits: (i) arbitrary backbone choice, including normal ($\beta = 0$) and lognormal ($\beta = 1$) backbones, (ii) availability of an approximate but fast vanilla options pricing method, and (iii) parsimonious and intuitive parameters. The comments on those merits are presented in order. Regarding the CEV backbone, the popularity of the SABR model is yet another indication that the lognormal backbone is not a one-fits-all solution. The normal SABR ($\beta = 0$) should not be confused with the continuous limit of $\beta \to 0^+$: while $\beta = 0$ allows negative prices, $\beta \to 0^+$ does not. Hagan et al. (2002) derives an approximate formula for the BSM-implied volatility, from which option price can be obtained through the BSM formula. It is worth noting the derivation was via the perturbation from normal diffusion, therefore the implied normal volatility is computed first, even for $\beta > 0$. Since this study is concerned with the normal SV model, normal volatility is more relevant. For reference, the normal volatility approximation (Hagan and Woodward 1999, Hagan et al. 2002) for the normal SABR is:

$$\begin{aligned} \sigma_n(\sigma_0, \alpha, \rho, K) &= \sigma_0 \left(\frac{\zeta}{\chi}\right) \left(1 + \frac{2 - 3\rho^2}{24}\alpha^2 T\right) \\ \text{where} \quad \zeta &= \frac{\alpha}{\sigma_0}(\bar{F}_T - K) \quad \text{and} \quad \chi = \log\left(\frac{\sqrt{1 - 2\rho\zeta + \zeta^2} - \rho + \zeta}{1 - \rho}\right), \end{aligned} \tag{8}$$

where K is the strike price and T time-to-expiry. The volatility approximation is an asymptotic expansion for small volatility variance $\alpha^2 T$ $(= S)$. Although the accuracy of the approximation noticeably deteriorates as $\alpha^2 T$ increases, the error is irrelevant for vanilla options pricing to the extent that the model parameters, σ_0, α, ρ with pre-determined β, are to be calibrated to observable option prices. In this sense, the implied volatility formula rather serves as an interpolation method for the volatility smile. The error causes serious issues only when the usage of the model goes beyond vanilla options pricing. Two important cases are (i) exotic options pricing, which requires the knowledge of probability density, and (ii) path-dependent claims, which require Monte Carlo (MC) simulation. In the first case, the probability density implied from the formula often results in negative density at out-of-the-money strikes, thus allowing for arbitrage. In the second case, the vanilla option price from the formula is not consistent with that from the MC simulation with the

same parameters. Therefore, the parameter calibration for MC scheme should be performed with extra care. As such, the literature on more accurate SABR solutions arrive after the SABR model establishes its popularity among practitioners. Below, we review prior work on the SABR model, particularly the normal case.

For vanilla options pricing, there have been various improvements to the implied volatility approximation (Obłój 2007, Lorig et al. 2015, Balland and Tran 2013, Wu 2012, Andersen and Brotherton-Ratcliffe 2005, Jordan and Tier 2011). The exact vanilla option price is known only for three special cases: (i) zero correlation ($\rho = 0$), (ii) lognormal SABR ($\beta = 1$), and (iii) normal SABR ($\beta = 0$). For the zero-correlation case, the price process can be transformed into the CEV process with the changed time scale of the integrated variance, $A^{[-1/2]}$. Therefore, the option price can be expressed by (multiple) integral over the option prices from the CEV model. See Antonov et al. (2013) for the most simplified integral representation based on the heat kernel on the two-dimensional hyperbolic geometry (McKean et al. 1970) (see below). The solution to the lognormal SABR is expressed in terms of Gaussian hypergeometric series (Lewis 2000). For the general cases (i.e., $\rho \neq 0$ and $0 < \beta < 1$), there is no analytic alternative to the finite difference method (Park 2014, Le Floc'h and Kennedy 2014). However, a further discussion is beyond the scope of this paper.

The normal SABR (and NSVh) model is closely related to the BM on hyperbolic geometry, represented as a Poincaré half-plane. We denote the n-dimensional Poincaré half-plane by $\mathbb{H}_n$. Table 1 is the *cheat sheet* for the properties of $\mathbb{H}_2$ and $\mathbb{H}_3$. The standard BM in a geometry is defined to be the stochastic process whose infinitesimal generator is given by Laplace-Beltrami operator Δ defined under the geometry. Heat kernel $p(t, D)$ is the fundamental solution of diffusion equation $(\partial_t - \frac{1}{2}\Delta)p(t, D) = 0$, thus the transition probability of the standard BM. The heat kernels on $\mathbb{H}_n$ has analytic solutions (see Grigor'yan and Noguchi (1998) for derivation). In Table 1, we show the heat kernels for $\mathbb{H}_2$ (McKean et al. 1970), often referred to as McKean kernels, and $\mathbb{H}_3$ (Debiard et al. 1976).

The standard BM on $\mathbb{H}_2$ corresponds exactly to the normal SABR with $\rho = 0$ in canonical form. Naturally, the $\mathbb{H}_2$ heat kernel has been used for the analysis of the normal SABR. Henry-Labordère (2005, 2008) expresses the vanilla option price under the normal SABR with a two-dimensional integral, although it is later corrected by Korn and Tang (2013). Antonov et al. (2015) further simplify the price to a one-dimensional integration with an accurate approximation. However, their approaches are limited in that they fail to provide efficient numerical methods with fast convergence, such as numerical quadrature or fast Fourier transform, nor are their approaches based on the $\mathbb{H}_2$ kernel useful for the simulation algorithm.

Table 1 Properties of the n-Dimensional Hyperbolic Geometry Represented by n-Dimensional Poincaré Half-Plane $\mathbb{H}_n$ for $n=2$ and 3. Symbols ∂_x and ∂_x^2 are the shortened notations for partial derivative operators $\frac{\partial}{\partial x}$ and $\frac{\partial^2}{\partial x^2}$, respectively.

Dimension	$\mathbb{H}_2=\{(x,z):z>0\}$	$\mathbb{H}_3=\{(x,y,z):z>0\}$
Metric $(ds)^2$	$(dx^2+dz^2)/z^2$	$(dx^2+dy^2+dz^2)/z^2$
Volume element dV	$dx\,dz/z^2$	$dx\,dy\,dz/z^3$
Geodesic distance D $(x,\cdot,z)$ to $(x',\cdot,z')$	$\operatorname{acosh}\left(\frac{(x'-x)^2+z^2+z'^2}{2zz'}\right)$	$\operatorname{acosh}\left(\frac{(x'-x)^2+(y'-y)^2+z'^2+z^2}{2zz'}\right)$
Laplace-Beltrami operator $\Delta_{\mathbb{H}_n}$	$z^2\left(\partial_x^2+\partial_z^2\right)$	$z^2\left(\partial_x^2+\partial_y^2+\partial_z^2\right)-z\,\partial_z$
Standard BM	$dx_t=z_t dX_t$, $dz_t/z_t=dZ_t$	$dx_t=z_t dX_t$, $dy_t=z_t dY_t$, $dz_t/z_t=dZ_t-dt/2$
Heat kernel $p_n(t,D)$ for $n=2$ or 3 $(\partial_t-\frac{1}{2}\Delta_{\mathbb{H}_n})p_n=0$	$\frac{\sqrt{2}e^{-t/8}}{(2\pi t)^{3/2}}\int_D^\infty ds\frac{se^{-s^2/2t}}{\sqrt{\cosh s-\cosh D}}$	$\frac{1}{(2\pi t)^{3/2}}\frac{D}{\sinh D}e^{-(t^2+D^2)/2t}$

The simulation methods of SABR dynamics have been recently developed. While several efficient approximations (Chen et al. 2012, Leitao et al. 2017a,b) have been proposed, Cai et al. (2017) develop a simulation method that is *exact* under three special cases: (i) $\rho=0$, (ii) $\beta=0$, and (iii) $\beta=1$. The key of this method is to simulate the time-integrated variance, conditional on terminal volatility $A_S^{[-1/2]}|Z_S$ from the CDF obtained from the Laplace transform of $(1/A_S^{[-1/2]})\,|\,Z_S$, which has a closed-form expression (Matsumoto and Yor 2005a). For the normal SABR, given the pair of Z_S and $A_S^{[-1/2]}$, (5) can be easily simulated using $X_{A_S^{[-1/2]}}\overset{d}{=}X_1\sqrt{A_S^{[-1/2]}}$ for a standard normal X_1. Although this method is exact in that the time-discretized Euler method is avoided, it comes at a heavy computation cost, that is, numerical inversion of the Laplace transform and root-solving for the CDF inversion.

On the other hand, our approach based on Alili and Gruet (1997) exploits the $\mathbb{H}_3$ heat kernel. Despite the added dimensionality, the $\mathbb{H}_3$ kernel is simpler in form than the $\mathbb{H}_2$ one. Furthermore, from the radial symmetry of (x_t,y_t), it is easy to extract x_t (or y_t) via cosine (or sine) projection. This approach works for both vanilla options pricing and MC simulation. Although our vanilla option price is expressed by a double integral, it can be evaluated with a numerical quadratures integral, thus being more efficient than the formula in (Henry-Labordère 2008, Korn and Tang 2013, Antonov et al. 2015). For MC simulation, we directly simulate $X_{A_S^{[\frac{1}{2}(\lambda-1)]}}$, conditional on Z_S in a closed-form expression. The advantage of using $\mathbb{H}_3$ is analogous to the two-dimensional normal density as the radial function being exploited for the evaluation of Gaussian integration $\int_{-\infty}^{\infty}e^{-x^2}dx=\sqrt{\pi}$ and the Box-Muller algorithm (Box and Muller 1958) for drawing normal random numbers.

2.3. Johnson's Distribution Family

Johnson (1949) proposes a system of distribution families in which a random variable X is represented by the following transformations from a standard normal variable Z:

$$\frac{X-\gamma_X}{\delta_X} = f\left(\frac{Z-\gamma_Z}{\delta_Z}\right) \quad \text{for} \quad f(x) = \begin{cases} 1/(1+e^{-x}) & \text{for } S_B \text{ (bounded) family} \\ e^x & \text{for } S_L \text{ (lognormal) family} \\ \sinh x & \text{for } S_U \text{ (unbounded) family,} \end{cases} \tag{9}$$

where γ_X and γ_Z are location parameters and δ_X and δ_Z scaling parameters. Although not explicitly included in the original manuscript, a normal distribution is also included in the systems, denoted by S_N with the trivial transformation $f(x) = x$. The range of X is unbounded for S_U and S_N, semi-bounded for S_L, and bounded for S_B. The system is designed such that a unique family is chosen, given a feasible pair of skewness and kurtosis. Given a fixed value for skewness, the kurtosis increases in the order of S_B, S_L, and S_U.

Particularly, the S_U distribution has been an attractive choice for modeling skewed and heavy-tailed distributions generalizing the normal distribution, and has been adopted in various fields. See Jones (2014) and the references therein. A few examples of applications in financial economics includes heavy-tailed innovation in the GARCH model (Choi and Nam 2008), accurate prediction of value-at-risk (Simonato 2011, Venkataraman and Rao 2016), and modeling returns of financial assets (Shang and Tadikamalla 2004, Corlu and Corlu 2015).

The merits of the S_U distribution are as follows. First, it explains a wide range of skewness and kurtosis. For a fixed value of skewness, it can accommodate arbitrary high values of kurtosis, which is not feasible in the classical approaches, such as the Gram-Charlier or Cornish-Fisher expansions. Second, many properties of the distributions are expressed in closed forms: probability and cumulative distribution functions and moments. Third, the parameters are efficiently estimated: see Tuenter (2001) for the reduced moment matching and Wheeler (1980) for the quantile-based estimation. Finally, it is trivial to sample random numbers, thus making S_U ideal for Monte-Carlo simulations, particularly in a multivariate setting (Biller and Ghosh 2006). Generally, sampling random numbers is not trivial, although the PDF is given in closed form.

Additionally, this study assigns a first-class-citizen status to the S_U distribution among other heavy-tailed distributions by showing it is a solution of a continuous-time SV process, that is, the NSVh model with $\lambda = 1$. This result relies on Alili et al. (1997). We thereby explain why the S_U distribution has been superior in estimating asset return distributions and risk metrics. The unlikely connection between S_U and the NSVh model is mutually beneficial (see § 3.3 for details). Furthermore, we numerically show the normal SABR ($\lambda = 0$) and S_U ($\lambda = 1$) are very close, thus can be used interchangeably for practical purposes. Therefore, the normal SABR can be replaced with the S_U distribution, which has closed-form option price (see § 4 for details).

3. Main Results

We begin by stating Bougerol (1983)'s identity in the original form. The proof is deferred to Proposition 3, which presents the more general result.

PROPOSITION 1 **(Bougerol's identity)**. *For a fixed time T, the followings are equal in the distribution:*

$$\int_0^T e^{Z_t} dX_t \overset{d}{=} X_{A_T} \overset{d}{=} \sinh(W_T), \tag{10}$$

where X_t, W_t and Z_t are independent BMs and $A_T = A_T^{[0]}$ is defined by (6).

This identity is surprising, in that the stochastic integral involving two independent BMs is equal to a sinh transformation of one BM in the distribution. See Matsumoto and Yor (2005a), Vakeroudis (2012) for a review and related topics. Note that the identity is valid as distribution at a fixed time $t = T$, not as a process for $0 \le t \le T$. Nevertheless, it does not directly help solve (5). The identity needs to be generalized to include drift in $A^{[\mu]}$ and provide the joint distribution with $Z^{[\mu]}$ for $\mu \neq 0$. Such generalizations are found in Alili and Gruet (1997) and Alili et al. (1997). Our main results are the direct consequences of the results.

3.1. Monte-Carlo Simulation Scheme

The first generalization is concerned with the identity of the distribution of $X_{A_T^{[\mu]}}$, conditional on $Z_T^{[\mu]}$, which is related to the BMs in $\mathbb{H}_3$. We restate Proposition 3 in Alili and Gruet (1997) in a slightly modified form:

PROPOSITION 2 **(Bougerol's identity in hyperbolic geometry)**. *Let X_t and Z_t be two independent BMs and the function ϕ defined by*

$$\phi(Z, D) = e^{Z/2}\sqrt{2\cosh D - 2\cosh Z} \quad \textit{for} \quad Z \le D. \tag{11}$$

Then, the following are equal in the distribution:

$$\int_0^T e^{Z_t^{[\mu]}} dX_t \overset{d}{=} X_{A_T^{[\mu]}} \overset{d}{=} \cos\theta\, \phi\left(Z_T^{[\mu]}, \sqrt{R_T^2 + (Z_T^{[\mu]})^2}\right), \tag{12}$$

where R_t is a two-dimensional Bessel process, that is, the radial part of a BM in two-dimensional Euclidean space, and θ is a uniformly distributed random angle. The three random variables, R_T, Z_T, and θ, are independent.

Proof Among the two proofs in Alili and Gruet (1997), we follow the one exploiting geometrical interpretation. We further simplify the original proof by use of the $\mathbb{H}_3$ heat kernel.

Let (x_t, y_t, z_t) be a three-dimensional hyperbolic BM with a drift on z-axis, started at $(x_0, y_0, z_0) = (0, 0, 1)$:

$$dx_t = z_t\, dX_t, \quad dy_t = z_t\, dY_t, \quad \text{and} \quad \frac{dz_t}{z_t} = dZ_t + \left(\frac{1}{2} + \mu\right) dt. \tag{13}$$

Obviously,

$$x_T \overset{d}{=} y_T \overset{d}{=} X_{A_T^{[\mu]}} \quad \text{and} \quad z_T = \exp\left(Z_T^{[\mu]}\right),$$

so drift μ is equivalent to $(\lambda-1)/2$ in NSVh model. The standard BM in $\mathbb{H}_3$ introduced in Table 1 corresponds to $\mu=\lambda=-1$. If we let D_t be the hyperbolic distance between (x_t, y_t, z_t) and starting point $(0,0,1)$,

$$D_t = \operatorname{acosh}\left(\frac{1}{2}\left(\frac{x_t^2+y_t^2}{z_t} + z_t + \frac{1}{z_t}\right)\right),$$

the function ϕ is related to the Euclidean radius of (x_t, y_t) by

$$r_t = \sqrt{x_t^2+y_t^2} = \phi\left(Z_t^{[\mu]},\, D_t\right). \tag{14}$$

The underlying BM, $Z_t^{[\mu]}$, can be also interpreted as the projection of (x_t, y_t, z_t) onto the z-axis, that is, the signed hyperbolic distance from $(0,0,1)$ to $(0,0,z_t)$. Therefore, restriction $Z_t^{[\mu]} \le D_t$ is naturally satisfied.

A critical step of the proof is to show, for a fixed time T,

$$D_T \overset{d}{=} \sqrt{X_T^2+Y_T^2+(Z_T^{[\mu]})^2} \quad \text{conditional on} \quad Z_T^{[\mu]}, \tag{15}$$

which effectively means that the hyperbolic distance between (x_T, y_T, z_T) and starting point $(0,0,1)$ has the same distribution as the Euclidean distance of the underlying BMs, $(X_T, Y_T, Z_T^{[\mu]})$, from $(0,0,0)$. Furthermore, the identity holds conditional on $Z_T^{[\mu]}$. Based on the identity, it follows that

$$\sqrt{x_T^2+y_T^2} \overset{d}{=} \phi\left(Z_T^{[\mu]},\, \sqrt{X_T^2+Y_T^2+(Z_T^{[\mu]})^2}\right),$$
$$x_T \overset{d}{=} \cos\theta\, \phi\left(Z_T^{[\mu]},\, \sqrt{X_T^2+Y_T^2+(Z_T^{[\mu]})^2}\right).$$

Proving (15) for just one value of μ is enough and the rest follows from Girsanov's theorem. To take advantage of the $\mathbb{H}_3$ heat kernel, we choose $\mu=-1$. From the derivative of (14), $r_T dr_T = z_T \sinh D_T dD_T$, the joint PDF on r_T and z_T is obtained from $p_3(t,D)$:

$$\text{Prob}(r_T \in dr_T, z_T \in dz_T) = p_3(T, D_T)\frac{2\pi r_T\, dr_T dz_T}{z_T^3} = \frac{1}{\sqrt{2\pi T^3}} D_T\, e^{-\frac{1}{2T}(T^2+D_T^2)}\frac{dD_T dz_T}{z_T^2}.$$

From $dz_T/z_T = dZ_T^{[-1]}$, we also know

$$\text{Prob}(z_T \in dz_T) = \frac{1}{\sqrt{2\pi T}} e^{-\frac{1}{2T}Z_T^2} \cdot \frac{dz_T}{z_T}.$$

Therefore, the conditional probability is given as

$$\text{Prob}(r_T \in dr_T | Z_T) = \frac{\text{Prob}(r_T \in dr_T, z_T \in dz_T)}{\text{Prob}(z_T \in dz_T)} = \frac{D_T}{T}\, e^{-\frac{1}{2T}\left(D_T^2+T^2-Z_T^2\right)}\frac{dD_T}{z_T} = \frac{D_T}{T}\, e^{-\frac{1}{2T}\left(D_T^2-(Z_T^{[-1]})^2\right)} dD_T.$$

The probability can be interpreted as the conditional probability $\text{Prob}(\sqrt{X_T^2+Y_T^2+(Z_T^{[-1]})^2} \in dD_T \,|\, Z_T)$. $\square$

Although not explicitly stated in the original manuscript, it is obvious from (15) that the identities hold conditional on $Z_T^{[\mu]}$. Therefore, Proposition 2 can be directly applied to the NSVh distribution of (5).

COROLLARY 1. *The joint distribution of the NSVh model at a fixed time S is given as*

$$\tilde{F}_S \stackrel{d}{=} \rho\left(e^{Z_S^{[\frac{1}{2}(\lambda-1)]}} - e^{\frac{1}{2}\lambda S}\right) + \rho_* \cos\theta\, \phi\left(Z_S^{[\frac{1}{2}(\lambda-1)]}, \sqrt{R_S^2 + (Z_S^{[\frac{1}{2}(\lambda-1)]})^2}\right), \tag{16}$$

and $\tilde{\sigma}_S = \exp\left(Z_S^{[\frac{1}{2}(\lambda-1)]}\right)$. Furthermore, from the independence of R_S and θ, we have the MC simulation as follows:

$$\left(Z_S, R_S^2, \cos\theta\right) \stackrel{d}{=} \left(Z_1\sqrt{S},\, (X_1^2+Y_1^2)S,\, \frac{X_1 \text{ (or } Y_1)}{\sqrt{X_1^2+Y_1^2}}\right), \tag{17}$$

where X_1 and Y_1 are independent standard normals.

Our simulation method using standard normals is more efficient than drawing R_S and θ from exponential and uniform distributions, respectively, as we avoid the costly computation of $\cos\theta$. Therefore, our MC method follows a similar idea to the Marsaglia polar method (Marsaglia and Bray 1964) for drawing normal random variables. Note that the three random numbers, X_1, Y_1, and Z_1, generate two draws of $\tilde{F}_S$. Therefore, one draw only requires one and a half (1.5) normal random variables. This is an unprecedented efficiency for any simulation method of SV models. For a special case of NSVh discussed in § 3.3, we achieve a one-to-one ratio. Although scheme (16) jumps directly from $s=0$ to $s=S$, it can be used for any time interval from $s=S_1$ to $s=S_2$ for $S_1 < S_2$.

3.2. Vanilla Option Price and Probability Density

The closed-form transition (16) also enables an efficient pricing method for vanilla options. The random variables, Z_S, R_S^2, and θ, follow closed-form PDFs, that is, normal, exponential, and uniform distributions, respectively. We can easily identify the integration range under which the payoff is positive. Given the values of Z_S and R_S, we identify the range of θ.

For numerically stable integration, we instead use the probability measure under which $Z_S^{[-1/2]}$ is a standard BM. The inverse Radon-Nikodym derivative $\exp(-\frac{1}{2}Z_S^{[-1/2]} - \frac{1}{8}S)$ mitigates and symmetrizes the exponential growth of the integrand to $\exp(\frac{1}{2}|Z_S|)$ as $|Z_S| \to \infty$, regardless of λ. Note that choice $Z_S^{[-1/2]}$ corresponds to drift parameter $\lambda = -1$, which is the standard BM in $\mathbb{H}_3$. Let $u = Z_S^{[-1/2]}/\sqrt{S}$ and $v = R_S^2/S - v_0$ for some $v_0 \geq 0$ we define below. Then, the probability densities around variables u, v, and θ are $e^{-\frac{1}{2}u\sqrt{S}-\frac{1}{8}S}n(u)du$, $e^{-\frac{1}{2}(v_0+v)}dv/2$, and $d\theta/\pi$, respectively.

We define the following functions:

$$g(u) = \rho\, e^{\frac{1}{2}\hat{u}\sqrt{S}} - \left(\rho e^{\frac{1}{2}\lambda S} + \frac{\alpha}{\sigma_0}(K - \bar{F}_T)\right) e^{-\frac{1}{2}\hat{u}\sqrt{S}},$$
$$h(u, v_0 + v) = \rho_* \left(2\cosh\sqrt{(v_0 + v + \hat{u}^2)S} - 2\cosh(\hat{u}\sqrt{S})\right)^{1/2} \quad (v \geq 0),$$

where $\hat{u} = Z_S^{[\frac{1}{2}(\lambda-1)]}/\sqrt{S} = u + \frac{1}{2}\lambda\sqrt{S}$ is introduced for simpler notation. Using g and h, the moneyness of an option with strike price K is expressed as

$$F_T - K = \frac{\sigma_0}{\alpha} e^{\frac{1}{2}\hat{u}\sqrt{S}} \left(g(u) + \cos\theta\, h(u, v_0 + v)\right).$$

Value v_0 is the root of $|g(u)| = h(u, v_0)$, so that $h(u, v_0 + v)\cos\theta_0 = |g(u)|$ can always have root θ_0 for any value $v \geq 0$. This is possible because function $h(u, \cdot)$ monotonically increases from 0 to ∞ regardless of u. Therefore, v_0 and θ_0 are expressed as functions of u and v:

$$v_0(u) = \frac{1}{S}\operatorname{acosh}^2\left(\cosh\left(\hat{u}\sqrt{S}\right) + \frac{g^2(u)}{2\rho_*^2}\right) - \hat{u}^2$$
$$\theta_0(u, v) = \arccos\left(\frac{|g(u)|}{h(u, v_0 + v)}\right).$$

The undiscounted price of vanilla options struck at K is expressed as a double integration:

$$\begin{aligned} V_\pm &= E\left(\max(\pm(F_T - K), 0)\right) \\ &= e^{\frac{1}{8}(1+\lambda)S}\frac{\sigma_0}{\alpha}\int_{u=-\infty}^{\infty} n(u)du \left(\max(\pm g, 0) + \int_{v=0}^{\infty} e^{-\frac{1}{2}(v_0+v)}\frac{dv}{2}\int_{\theta=0}^{\theta_0}\frac{d\theta}{\pi}(-|g| + h\cos\theta)\right) \\ &= e^{\frac{1}{8}(1+\lambda)S}\frac{\sigma_0}{\alpha}\int_{u=-\infty}^{\infty} n(u)du \left(\max(\pm g, 0) + e^{-\frac{v_0}{2}}\int_{v=0}^{\infty} e^{-\frac{v}{2}}\frac{dv}{2\pi}\left(-|g|\,\theta_0 + \sqrt{h^2 - g^2}\right)\right), \end{aligned} \tag{18}$$

where the call option price is denoted by V_+ and the put option by V_-.

This integration can be efficiently evaluated with numeral quadratures. We use the Gauss-Hermite quadrature associated with weight $n(u)$ for u and the generalized Gauss-Laguerre quadrature associated with weight $\sqrt{v}\,e^{-v/2}$ for v. We include $\sqrt{v}$ to accurately capture the cusp of integrand $(-|g|\,\theta_0 + \sqrt{h^2 - g^2}) \sim \sqrt{v}$ for small v. Total node size is the product of each quadrature size $M = M_1\, M_2$, where M_1 and M_2 are discretization sizes for u and v, respectively. In the pricing of ATM options ($K = \bar{F}_T$), under the normal SABR ($\lambda = 0$), which is the most frequent usage, we can use $u = \hat{u}$ and the symmetries on u, $g(u) = -g(-u)$, and $h(u, v) = h(-u, v)$, so the size of quadrature nodes can be halved. For this reason, it is better to choose M_1 as an even number.

The cumulative probability density at (or the price of undiscounted binary put options struck at) K is similarly obtained as

$$P_\lambda(K) = e^{-\frac{1}{8}S}\int_{u=-\infty}^{\infty} n(u)du\, e^{-\frac{1}{2}u\sqrt{S}}\left(\frac{1 - \operatorname{sgn}(g)}{2} + \operatorname{sgn}(g)\, e^{-\frac{v_0}{2}}\int_{v=0}^{\infty} e^{-\frac{v}{2}}\frac{dv}{2\pi}\theta_0\right), \tag{19}$$

where $\operatorname{sgn}(\cdot)$ is the sign function. The evaluation can be similarly done with the quadratures described above.

3.3. S_U Distributions for $\lambda = 1$

We now show that the NSVh distribution for $\lambda = 1$ is expressed by the S_U distribution and is related to Bougerol's identity generalized to an arbitrary starting point. In the following proposition, we restate Proposition 4 of Alili and Gruet (1997) (or Theorem 3.1 of Matsumoto and Yor (2005a)). More general results are found in Proposition 1 of Alili et al. (1997) (or Proposition 2.1 of Vakeroudis (2012)), and we follow the proof therein.

PROPOSITION 3 **(Bougerol's identity with an arbitrary starting point)**. *For a fixed time T and independent BMs, X_t, Z_t and W_t, the following are equal in the distribution:*

$$\sinh(a)\, e^{Z_T} + \int_0^T e^{Z_t} dX_t \overset{d}{=} \sinh(a)\, e^{Z_T} + X_{A_T} \overset{d}{=} \sinh(W_T + a). \tag{20}$$

Proof The following two processes

$$P_t = \sinh(W_t + a) \quad \text{and} \quad Q_t = e^{Z_t}\left(\sinh(a) + \int_0^t e^{-Z_s} dX_s\right),$$

are equivalent because the SDEs are the same with the same starting point, $P_0 = Q_0 = \sinh(a)$:

$$dP_t = \frac{1}{2} P_t dt + \sqrt{1 + P_t^2}\, dW_t \quad \text{and} \quad dQ_t = \frac{1}{2} Q_t dt + dX_t + Q_t\, dZ_t \overset{d}{=} \frac{1}{2} Q_t dt + \sqrt{1 + Q_t^2}\, dW_t.$$

Therefore, P_t and Q_t have the same distribution for any time t. For a fixed time T, $Z_T - Z_{T-s}$ for $0 \le s \le T$ is also a standard BM with the same ending point Z_T. By the time reversal $s \to T - s$, Q_T and the left-most term of (20) are equal in the distribution. □

The original Bougerol's identity of Proposition 1 is a special case, with $a = 0$. Now, Proposition 3 can be applied to derive the NSVh distribution for $\lambda = 1$.

COROLLARY 2. *The NSVh distribution for $\lambda = 1$ at a fixed time S is given by a re-parametrized S_U distribution:*

$$\tilde{F}_S \overset{d}{=} \rho_* \sinh\left(W_S + \operatorname{atanh} \rho\right) - \rho\, e^{S/2}, \tag{21}$$

or equivalently by a simpler form:

$$\tilde{F}_S \overset{d}{=} \sinh(W_S) + \rho\left(\cosh(W_S) - e^{S/2}\right). \tag{22}$$

Proof We use the following hyperbolic function identities,

$$\operatorname{asinh}\left(\frac{\rho}{\rho_*}\right) = \operatorname{atanh} \rho = \frac{1}{2} \log\left(\frac{1+\rho}{1-\rho}\right).$$

The rest of the proof is trivial. □

From the simulation perspective, Corollary 2 is even more efficient than Corollary 1, although for a special case $\lambda = 1$. However, this is at the expense of the conditional volatility state Z_S being

lost. While Corollary 1 can generate the path of price F_{t_k} for a discrete set of $0 \le t_k \le T$, Corollary 2 can only generate final price F_T.

The far more important consequence of Corollary 2 is that it bridges the S_U and NSVh model SDEs, which have been considered unrelated. Although Proposition 3 is a well-known result, to the best of our knowledge, this is the first time the result is recognized in the context of the S_U distribution and SV model, which is mutually beneficial.

First, the NSVh model gives a better parametrization of the S_U distribution than the original in (9). The two sets of parameters are interchanged by

$$\delta_Z = \frac{1}{\sqrt{S}}, \quad \frac{\gamma_Z}{\delta_Z} = -\operatorname{atanh}\rho, \quad \delta_X = \frac{\sigma_0\rho_*}{\alpha}, \quad \text{and} \quad \gamma_X = \bar{F}_T - \frac{\sigma_0\rho}{\alpha}e^{S/2}.$$

Note that this is the one-to-one mapping between parameter sets $\{(\delta_Z > 0, \gamma_Z, \delta_X > 0, \gamma_X)\}$ and $\{(\bar{F}_T, \sigma_0/\alpha > 0, S > 0, \rho)\}$. NSVh parameters are more intuitive. From the simpler form (22), the symmetric heavy tail comes from the sinh term, controlled by S, and the asymmetric skewness from the cosh term, controlled by ρ. The new parametrization also helps understand the relationship between Johnson family members. The lognormal family S_L is recognized as a special case with $\rho = \pm 1$ ($\rho_* = 0$) as $\tilde{F}_S \overset{d}{=} \pm\,(e^{Z_S} - e^{S/2})$. The normal family S_N is obtained as $\tilde{F}_S/\sqrt{S}$ in the limit of $S \to 0$ from linearization $\tilde{F}_S \approx W_S + (\rho/2)(W_S^2 - S)$ for small S.

Conversely, the S_U distribution provides analytic tractability to the NSVh model. Below are the closed-form expressions for the quantities of interest:

- PDF, $p_{\lambda=1}(x)$, and CDF, $P_{\lambda=1}(x)$:

$$p_{\lambda=1}(x) = \frac{n(d)}{\rho_*\sigma_0\sqrt{T}\sqrt{1+\xi^2}}m \quad \text{and} \quad P_{\lambda=1}(x) = N(-d)$$
$$\text{where} \quad \xi = \frac{\alpha}{\rho_*\sigma_0}(\bar{F}_T - x) - \frac{\rho}{\rho_*}e^{S/2}, \quad d = \frac{1}{\sqrt{S}}\left(\operatorname{asinh}\xi + \operatorname{atanh}\rho\right).$$

- The undiscounted price of vanilla option price struck at K ($\pm$ indicates call/put options respectively):

$$V_\pm = \frac{\sigma_0}{2\alpha}e^{S/2}\left((1+\rho)N(d+\sqrt{S}) - (1-\rho)N(d-\sqrt{S}) - 2\rho N(d)\right) \pm \left(\bar{F}_T - K\right)N(\pm d),$$
$$\text{where} \quad d = \frac{1}{\sqrt{S}}\left(\operatorname{asinh}\left(\frac{\alpha}{\rho_*\sigma_0}(\bar{F}_T - K) - \frac{\rho}{\rho_*}e^{S/2}\right) + \operatorname{atanh}\rho\right). \tag{23}$$

- Value-at-risk (VaR):

$$\mathrm{VaR}(q) = \bar{F}_T + \frac{\sigma_0}{\alpha}\left(\rho_*\sinh\left(\sqrt{S}Z_q + \operatorname{atanh}\rho\right) - \rho\, e^{S/2}\right) \quad \text{for} \quad Z_q = N^{-1}(q).$$

- Expected shortfall (ES):

$$\mathrm{ES}(q) = \bar{F}_T + \frac{\sigma_0 e^{S/2}}{2\alpha q}\left((1+\rho)N(Z_q - \sqrt{S}) - (1-\rho)N(Z_q + \sqrt{S}) - 2\rho q\right) \quad \text{for} \quad Z_q = N^{-1}(q).$$

The presented PDF and CDF are merely a re-parametrization of those under the S_U distribution, while the rest are new. Note that the vanilla option price is given by a closed-form solution (23), which is unprecedented in the literature on SV. The exact option value will serve as a benchmark to measure the accuracy of the numerical method in § 3.2 (see § 4).

3.4. Moments Matching of the NSVh Distribution

We derive the first four moments, skewness, and ex-kurtosis parameters of the NSVh distribution. The result can be used for the parameter estimations from samples and parameter conversion between the normal SABR ($\lambda = 0$) and S_U ($\lambda = 1$).

The moments conditional on $Z_T^{[\mu]}$ is given by

$$\begin{aligned} E\Big(X_{A_T^{[\mu]}}^{2n}\Big|Z_T^{[\mu]}\Big) &= E(\cos^{2n}\theta)\, E\left(\phi^{2n}\left(Z_T^{[\mu]},\, \sqrt{X_T^2+Y_T^2+(Z_T^{[\mu]})^2}\right)\right) \\ &= \frac{(2n-1)!!}{n!} T^n\, e^{nu\sqrt{T}} \int_u^\infty r e^{-\frac{1}{2}r^2} \Big(\cosh(r\sqrt{T}) - \cosh(u\sqrt{T})\Big)^n\, dr, \end{aligned}$$

where $u = |Z_T^{[\mu]}|/\sqrt{T}$ and $(2n-1)!! = (2n-1)(2n-3)\cdots 3\cdot 1$. This formula is comparable to the formula for $E\Big(\big(A_T^{[\mu]}\big)^n\Big|Z_T^{[\mu]}\Big)$ given in Proposition 5.3 in Matsumoto and Yor (2005a). The first two values are computed in closed form:

$$\begin{aligned} E\Big(X_{A_T^{[\mu]}}^{2}\Big|Z_T^{[\mu]}\Big) &= T e^{u\sqrt{T}} m(u,\sqrt{T}) \\ E\Big(X_{A_T^{[\mu]}}^{4}\Big|Z_T^{[\mu]}\Big) &= 3T^2 e^{2u\sqrt{T}} \Big(m(u,2\sqrt{T}) - \cosh(u\sqrt{T})\, m(u,\sqrt{T})\Big) \\ \text{where}\quad m(u,\epsilon) &= \frac{N(u+\epsilon)-N(u-\epsilon)}{2\epsilon\, e^{-\frac{1}{2}\epsilon^2}\, n(u)}. \end{aligned}$$

From these, the first two conditional moments of $A_T^{[\mu]}$ are trivially obtained as $E\Big(A_T^{[\mu]}\Big|Z_T^{[\mu]}\Big) = E\Big(X_{A_T^{[\mu]}}^{2}\Big|Z_T^{[\mu]}\Big)$ and $E\Big(\big(A_T^{[\mu]}\big)^2\Big|Z_T^{[\mu]}\Big) = \frac{1}{3}E\Big(X_{A_T^{[\mu]}}^{4}\Big|Z_T^{[\mu]}\Big)$, and the result matches that of Kennedy et al. (2012).

The unconditional moments of $X_{A_S^{[\mu]}}$ are given as

$$\begin{aligned} E\Big(X_{A_S^{[\mu]}}^{2}\Big) &= \frac{w^{2+2\mu}-1}{2+2\mu} \\ E\Big(X_{A_S^{[\mu]}}^{4}\Big) &= \frac{3}{2}\left(-w^{2+2\mu}\,\frac{w^{6+2\mu}-1}{6+2\mu} + (w^{4+2\mu}+1)\frac{w^{4+2\mu}-1}{4+2\mu} - \frac{w^{2+2\mu}-1}{2+2\mu}\right), \end{aligned}$$

where $w = e^S$. Finally, the moments of the canonical NSVh distribution, $\tilde{\mu}_n = E(\tilde{F}_S^n)$ for $2 \le n \le 4$, are given as

$$\begin{aligned}
\tilde{\mu}_2 =& \rho^2\, w^\lambda (w-1) + \rho_*^2\, \frac{w^{1+\lambda}-1}{1+\lambda}, \\
\tilde{\mu}_3 =& \rho^3\, w^{\frac{3}{2}\lambda}(w-1)^2(w+2) + 3\rho\rho_*^2\, w^{\frac{1}{2}\lambda} \left(\frac{w^{3+\lambda}-1}{3+\lambda} - \frac{w^{1+\lambda}-1}{1+\lambda} \right), \quad \text{and} \\
\tilde{\mu}_4 =& \rho^4\, w^{2\lambda}(w-1)^2(w^4+2w^3+3w^2-3) + 6\rho^2\rho_*^2\, w^\lambda \left(w\, \frac{w^{5+\lambda}-1}{5+\lambda} - 2\, \frac{w^{3+\lambda}-1}{3+\lambda} \right. \\
& \left. + \frac{w^{1+\lambda}-1}{1+\lambda} \right) + \frac{3}{2}\rho_*^4 \left(-w^{1+\lambda}\, \frac{w^{5+\lambda}-1}{5+\lambda} + (w^{3+\lambda}+1) \frac{w^{3+\lambda}-1}{3+\lambda} - \frac{w^{1+\lambda}-1}{1+\lambda} \right).
\end{aligned} \tag{24}$$

The central moments of the original form can be scaled as $\mu_n = (\sigma_0/\alpha)^n \tilde{\mu}_n$, and the skewness and ex-kurtosis parameters are given as $s = \tilde{\mu}_3/\tilde{\mu}_2^{3/2}$ and $\kappa = \tilde{\mu}_4/\tilde{\mu}_2^2 - 3$, respectively. The obtained expressions generalize those for the special cases: S_L (lognormal) distribution ($\rho = \pm 1$) and S_U ($\lambda = 1$). Particularly, the moments for the normal SABR ($\lambda = 0$) are reported for the first time. With $\lambda = 0$, the variance, skewness, and ex-kurtosis can be further simplified as

$$\tilde{\mu}_2 = w - 1, \quad s = \rho(w+2)\sqrt{w-1}, \quad \kappa = (w-1)\left(\left(\frac{4\rho^2+1}{5} \right)(w^3+3w^2+6w+5) + 1 \right). \tag{25}$$

In Figure 1, we plot the contours of skewness and ex-kurtosis for various ρ and S. While the ex-kurtosis is attributed by S, skewness is explained by ρS rather than ρ itself. Therefore, we plot the contours on the plane of $(\rho S, S)$. As implied from the S_U curve, the range the ex-kurtosis NSVh distribution can produce is unbounded. While the contours for $\lambda = 1$ (S_U) and $\lambda = 0$ (normal SABR) are similar, the parameters for $\lambda = 0$ is slightly higher (in absolute terms for ρ) than those for $\lambda = 1$ as to obtain the same skewness and ex-kurtosis levels.

In parallel to Tuenter (2001)'s reduced moment matching method for the S_U distribution, we also develop a similar method for the normal SABR. Combined with Tuenter (2001), it can be used to quickly find the equivalent parameter sets calibrated to the same moments. By joining the s and κ of (25) via ρ, we express κ as a univariate function on $w \ge 1$

$$f(w) = \frac{4s^2(w^3+3w^2+6w+5)}{5(w+2)^2} + (w-1)\left(1 + \frac{1}{5}(w^3+3w^2+6w+5) \right), \tag{26}$$

For which we can numerically find the root w_* of $\kappa = f(w_*)$. The first term of (26) can be algebraically proven to be monotonically increasing for $w \ge 1$, thus so is $f(w)$. Therefore, we have a unique root, if it exists. We can further bound w_* by $w_m \le w_* \le w_M$ to expedite the numerical root-finding. Lower bound w_m is the unique cubic root of $s^2 = (w-1)(w+2)^2$ (the $\rho^2 = 1$ case) with $w \ge 1$:

$$w_m = 2\cosh\left(\frac{1}{3}\operatorname{acosh}\left(1 + \frac{s^2}{2} \right) \right).$$

Figure 1 Contour Plot of Skewness (Dashed Line, Red) and Excess Kurtosis (Solid Line, Blue) for Varying $S(=\alpha^2 T)$ versus ρS. The upper-left triangle $(\rho S, S)$ is for $\lambda=1$ (S_U) and the lower-right triangle $(S, \rho S)$ for $\lambda=0$ (normal SABR). The values for skewness are 0, 1.5, 3, 4.5, 6, and 8 and those for ex-kurtosis are 2, 7, 16, 40, 100, and 200 from the lower-left to the upper-right corner.

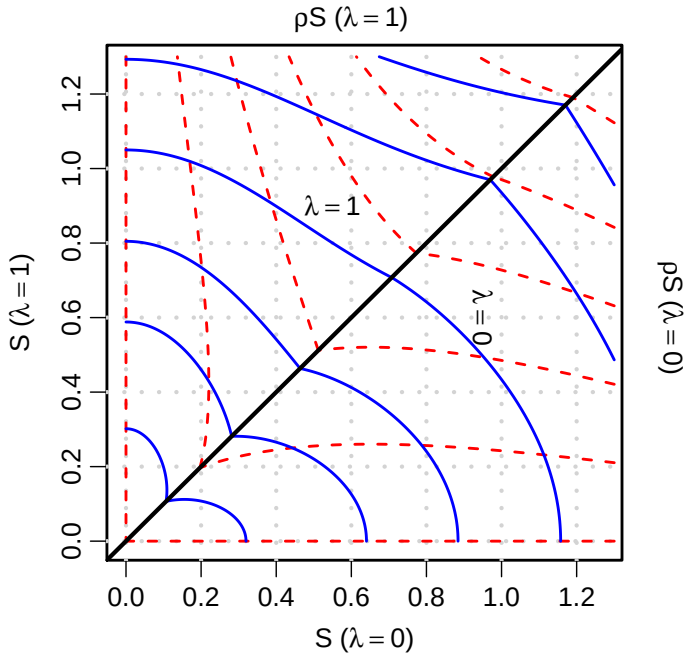

Upper bound w_M is obtained by plugging $w=w_m$ into (26), except the $(w-1)$ term:

$$w_M = 1 + \frac{\kappa - \frac{4}{5}s^2(w_m^3+3w_m^2+6w_m+5)/(w_m+2)^2}{1+\frac{1}{5}(w_m^3+3w_m^2+6w_m+5)}.$$

The existence of w_* is ensured by $f(w_m)\le\kappa$. If w_* exists and is found, the parameters can be solved as

$$S=\log w_*, \quad \rho=\frac{s}{(w_*+2)\sqrt{w_*-1}}, \quad \text{and} \quad \frac{\sigma_0}{\alpha}=\sqrt{\frac{\mu_2 \log w_*}{(w_*-1)S}}.$$

In Table 2, we summarize our results for the three important drift values, $\lambda=-1$, 0, and 1, for comparison.

4. Parameter Estimation from Empirical Data

Here, we calibrate the NSVh distribution to two empirical datasets: swaption volatility smile and daily stock index return. The purpose of this exercise is demonstrating various numerical procedures rather than arguing the NSVh model is superior to other SV models or heavy-tailed distributions in fitting these data. Additionally we show the two important NSVh models, $\lambda=0$ (normal SABR) and $\lambda=1$ (S_U), yield very similar distributions if calibrated to the same target (e.g., implied volatility or moments). Therefore, they can be used interchangeably.

Table 2 Summary of NSVh Model for the Three Key Drift Values: $\lambda = -1, 0$, and 1.

Drift parameter	$\lambda = -1$	$\lambda = 0$	$\lambda = 1$
Related topics	standard BM in $\mathbb{H}_3$ heat kernel $p_3(t, D)$	normal SABR (martingale)	S_U distribution
Drifted BM for $\tilde{\sigma}_s$	$Z_s^{[-1/2]}$	Z_s	$Z_s^{[1/2]}$
Terminal volatility $\tilde{\sigma}_S$	$\exp(Z_S^{[-1]})$	$\exp(Z_S^{[-1/2]})$	$\exp(Z_S)$
Integrated variance	$A_S^{[-1]}$	$A_S^{[-1/2]}$	$A_S (= A_S^{[0]})$
Exact simulation	Corollary 1		Corollary 2
Vanilla option price	Quadrature integral (18)		(23)
Moments	(24)		
Reduced moment matching		(26)	Tuenter (2001)

Figure 2 Swaption Volatility Smile in Normal Implied Volatility Observed on the US Market on March 14, 2017: (a) one year into one-year swap (1y1y) and (b) 10 years into 10-year swap (10y10y). While the circles are the volatilities implied from observed market prices, the three black circles indicate ATM and ATM $\pm$ 1% point, which are used for calibration. The solid line represents $\lambda = 1$ (S_U), the dashed one $\lambda = 0$ (normal SABR), the dotted the asymptotic expansion (8) for the normal SABR model.

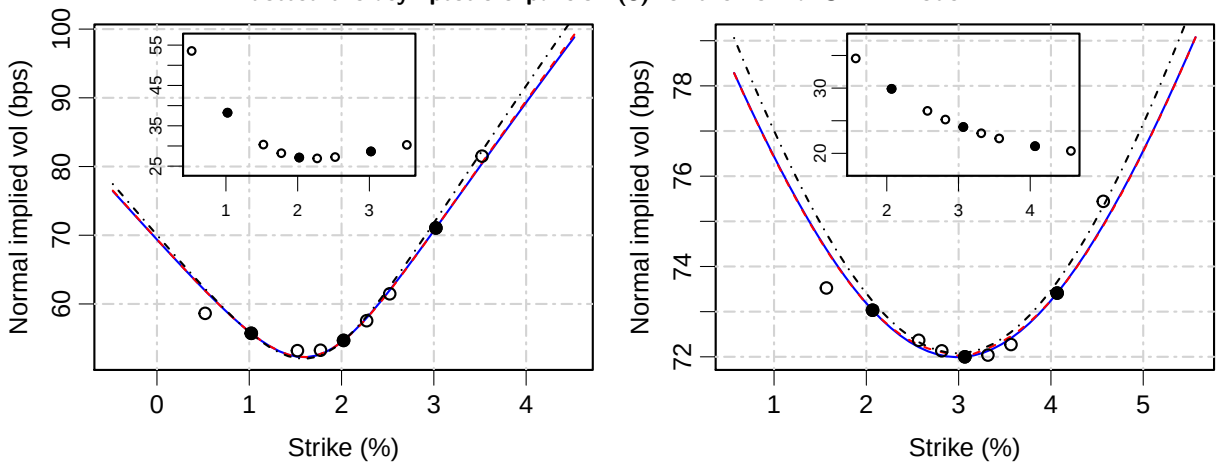

4.1. Swaption Volatility Smile

We calibrate the NSVh model to the US swaption market prices on March 14, 2017 from Reuters. The two heavily traded expiry—tenor pairs of US swaption, 1y1y and 10y10y, are chosen to illustrate different volatility smile shapes. To avoid the complication of annuity of the underlying swap, we compute the price in the unit of annuity from the BSM implied volatilities provided by Reuters, rather than raw dollar prices. See the insets of Figure 2 for the BSM implied volatilities.

Figure 2 shows the results of the calibration in normal volatility and Table 3 the calibrated parameter values for $\lambda = 0$ and $\lambda = 1$. While option prices are given for strike prices with spreads of ± 150, ± 100, ± 50, ± 25, and 0 basis points from the forward swap rates $\bar{F}_T$ (denoted by the circles in the plot), we only use the three spreads, -100, 0, $+100$ basis points (denoted by the

Table 3 Parameters Calibrated to the US Swaption Volatility Smile on March 14, 2017. See Figure 2 for the volatility smile and calibration points.

Parameters	1y1y ($T=1$)		10y10y ($T=10$)	
	$\lambda=0$	$\lambda=1$	$\lambda=0$	$\lambda=1$
ρ (%)	35.280	32.244	1.811	1.580
α (%)	64.634	62.181	23.535	22.196
σ_0 (%)	0.532	0.477	0.689	0.609
$\bar{F}_T$ (%)	2.0221		3.0673	

filled circles), so that the calibrated parameter set, (σ_0, α, ρ), reproduces option prices at the three strike prices. Note that the two volatility smile curves (solid blue and dashed red) implied from the calibrated models, $\lambda=0$ and $\lambda=1$, are almost indistinguishable, indicating similarity in the distributions. Therefore, this reconfirms the possibility of $\lambda=1$ being used as an alternative to the normal SABR ($\lambda=0$).

In Table 4, we show the accuracy of the option prices obtained from the quadratures integration in § 3.2 and the MC simulation (§ 3.1). To take advantage of the analytic option prices of (23), we choose the calibrated parameter values for $\lambda=1$ in Table 3. and measure errors from the exact prices. The exact prices are purely computed from the calibrated parameters, thus different from the observed market prices for the off-calibration strike. The prices from the quadratures method shows good accuracy: 128 (8×16) quadrature nodes yields errors in the order of 10^{-6}. The MC simulation with 10^5 samples (i.e., generated from 1.5×10^5 normal random numbers) have errors in the order of 10^{-5}. We observe a similar performance of our methods for the normal SABR ($\lambda=0$) model. Since exact prices are not available in this case, we obtain the converged price by increasing quadrature sizes. Our method also reconfirms the exact prices of the two test cases in Korn and Tang (2013).

4.2. Daily Return of Stock Index

We fit the NSVh distribution to the daily returns of two stock indices: US Standard & Poor's 500 Index (S&P 500) and China Securities Index 300 (CSI 300). The data cover the 12-year period from the beginning of 2005 to the end of 2016. To simplify the analysis and make it reproducible, daily returns are computed from the values of the outright indices, rather than total return indices.

The statistics of the daily returns are summarized in Table 5. Note that S&P 500 shows heavier tails but less skewness than CSI 300. The NSVh distribution is fitted to the first four moments for $\lambda=0$ and 1, for which the reduced moment-matching of Tuenter (2001) and ours in § 3.4 are respectively used. Table 6 shows the calibrated parameters. Based on these values, VaR and ES are computed and compared to those from the normal distribution assumption and the true values in the dataset. Table 7 shows the result. Overall, the VaR and ES from the fitted NSVh distributions

Table 4 **Accuracy of Vanilla Options Pricing § 3.2 Tested against the $\lambda = 1$ Parameters of Table 3. We evaluate the numerical integration with quadrature sizes, $M = 128\,(M_1 = 8, N_2 = 16)$ and measure the error from the analytic prices for $\lambda = 1$, evaluated by (23). The mean square error of the Monte-Carlo simulation (MC-MSE) is measured from 100 simulation runs with $100,000$ paths. Prices are in the unit of the annuity of the underlying swap.**

$K - F_T$	1y1y			10y10y		
(bps)	Price (%)	Error	MC-MSE	Price (%)	Error	MC-MSE
-150	1.5016	-4.0E-11	2.1E-5	1.8726	1.2E-6	5.9E-5
-100	1.0080	9.6E-12	2.0E-5	1.5059	3.5E-6	5.7E-5
-50	0.5473	5.0E-9	1.8E-5	1.1823	9.8E-6	5.4E-5
-25	0.3582	7.3E-7	1.7E-5	1.0387	1.3E-5	5.3E-5
0	0.2180	1.9E-6	1.4E-5	0.9078	3.5E-6	5.1E-5
25	0.1272	1.1E-6	1.2E-5	0.7899	1.1E-5	4.9E-5
50	0.0736	2.5E-7	9.5E-6	0.6847	9.3E-6	4.7E-5
100	0.0256	7.3E-8	5.9E-6	0.5103	3.9E-6	4.3E-5
150	0.0097	6.7E-8	3.7E-6	0.3781	1.6E-6	3.9E-5

Table 5 **Statistics of Daily Returns of S&P 500 and CSI 300 Indices from 2005 to 2016. The number of samples, k-th (central) moment, skewness, and ex-kurtosis are denoted by N, μ_k, s, and κ, respectively. The moments are computed from percent returns.**

	S&P 500	CSI 300
N	3020	2914
$\bar{F}_T$	0.0282	0.0417
μ_2	1.5154	3.4092
μ_3	-0.1741	-3.1949
μ_4	33.1731	73.6293
s	-0.0933	-0.5075
κ	11.4454	3.3348

Table 6 **Parameters Fitted to the Moments of Daily Returns of Stock Indices. We assume $T = 1$.**

Parameters	S&P 500		CSI 300	
	$\lambda = 0$	$\lambda = 1$	$\lambda = 0$	$\lambda = 1$
$\rho\,(\%)$	-2.042	-1.725	-20.454	-18.539
$\alpha\,(\%)$	88.533	84.587	63.782	61.853
$\sigma_0\,(\%)$	99.915	82.538	166.213	150.167

Table 7 **VaR and ES from Normal Distribution (Normal), the Two NSVh Distributions ($\lambda = 0$ and $\lambda = 1$), and the True Values from the Dataset (Sample).**

Risk Measures	S&P 500				CSI 300			
	Normal	$\lambda = 0$	$\lambda = 1$	Sample	Normal	$\lambda = 0$	$\lambda = 1$	Sample
VaR ($q = 5\%$)	-1.997	-1.825	-1.824	-1.832	-2.995	-3.032	-3.036	-3.007
VaR ($q = 1\%$)	-2.836	-3.405	-3.432	-3.615	-4.254	-5.234	-5.246	-5.732
ES ($q = 5\%$)	-2.511	-2.858	-2.872	-3.042	-3.767	-4.434	-4.440	-4.745
ES ($q = 1\%$)	-3.253	-4.784	-4.820	-5.309	-4.879	-6.853	-6.857	-7.298

Figure 3 Normal QQ Plots of Daily returns of the S&P 500 (left) and CSI 300 Indexes (right). The sample Z-score in y-axis is plotted against the Z-score from the normal distribution (black dot) and the $\lambda=1$ S_U ($\lambda=1$) distribution (green circle). The QQ plot between the two theoretical distributions from $\lambda=0$ and 1 (dashed red) is indistinguishable from the $y=x$ line (solid blue).

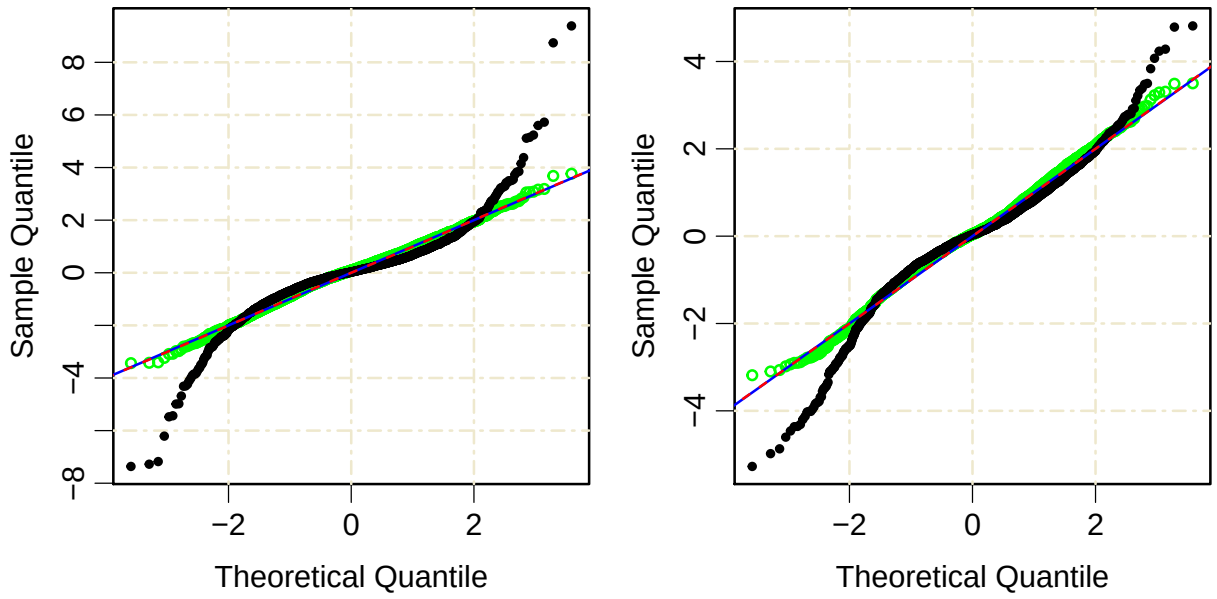

are much closer to the true values than those from the normal distribution. Note that the values from $\lambda=0$ and 1 are very close, indicating the similarity between the two distributions.

Further, we compare the goodness-of-fit of the S_U ($\lambda=1$) to that of the normal distribution using a normal quantile–quantile (QQ) plot. In Figure 3, the theoretical Z-score, $Z_y^{(j)}=N^{-1}(\frac{1}{N}(j-1/2))$ for the j-th sample, is shown on the x-axis and two different sample Z-scores on the y-axis: (i) from the estimated normal distribution, $Z_x^{(j)}=(X_j-\bar{F}_T)/\sqrt{\mu_2}$, as dots (black) and (ii) from the S_U distribution as circles (green) computed by

$$Z_x^{(j)}=N^{-1}(F_{\lambda=1}(X_j))=\frac{1}{\sqrt{S}}\left(\operatorname{asinh}\left(\frac{\alpha}{\rho_*\sigma_0}(X_j-\bar{F}_T)+\frac{\rho}{\rho_*}e^{S/2}\right)-\operatorname{atanh}\rho\right).$$

Finally, we also show the normal QQ plot of the two NSVh for $\lambda=0$ and 1 to demonstrate the closeness of the two distributions. The Z-score from the normal SABR ($\lambda=0$), $Z_y=N^{-1}(F_{\lambda=0}(X))$, on the y-axis is plotted versus the Z-score from the S_U ($\lambda=0$), $Z_x=N^{-1}(F_{\lambda=1}(X))$ on the x-axis. The QQ line (dashed red) is difficult to distinguish from the identity $y=x$ line (solid blue), indicating the two distributions are practically the same.

5. Conclusion

We consider a class of normal SV models, which serves as a derivative pricing model for assets such as interest rate and as a generator for heavy-tailed distributions. We provide tools to utilize the model, such as the closed-form simulation method, efficient numerical options pricing method,

and closed-form moments. The two important special cases of the hyperbolic normal SV model are the normal SABR ($\lambda = 0$) and the S_U distribution ($\lambda = 1$), thereby connecting the two seemingly unrelated topics. Numerical examples further demonstrate the distributions from the two cases are similar, so Johnson's S_U can serve as a fully analytic option valuation model. We estimate the model parameters for two empirical datasets: US swaption and daily returns distribution of the US S&P 500 and CSI 300 indexes.

Acknowledgments

The authors are grateful to Larbi Alili for sharing manuscripts Alili and Gruet (1997) and Alili et al. (1997). Jaehyuk Choi would like to thank his previous employer, Goldman Sachs, for the motivation of this study. The research of Byoung Ki Seo was supported by the "Human Resources Program in Energy Technology" from the Korea Institute of Energy Technology Evaluation and Planning (KETEP), funded by the Ministry of Trade, Industry and Energy, Republic of Korea (No. 20164010201030).

References

Alili, Larbi, Daniel Dufresne, Marc Yor. 1997. Sur l'identité de Bougerol pour les fonctionnelles exponentielles du mouvement brownien avec drift. Yor (1997), 3–14.

Alili, Larbi, J. C. Gruet. 1997. An explanation of a generalized Bougerol's identity in terms of hyperbolic Brownian motion. Yor (1997), 15–33.

Andersen, Leif BG, Rupert Brotherton-Ratcliffe. 2005. Extended libor market models with stochastic volatility. *Journal of Computational Finance* **9**(1) 1–40.

Antonov, Alexander, Michael Konikov, Michael Spector. 2013. SABR spreads its wings. *Risk* **August** 58.

Antonov, Alexandre, Michael Konikov, Michael Spector. 2015. Mixing SABR models for negative rates. *Available at SSRN* URL `https://ssrn.com/abstract=2653682`.

Bachelier, L. 1900. Théorie de la spéculation. *Annales Scientifiques de L'Ecole Normale Supérieure* **17** 21–88.

Badrinath, Swaminathan G, Sangit Chatterjee. 1988. On measuring skewness and elongation in common stock return distributions: The case of the market index. *Journal of Business* 451–472.

Balland, Philippe, Quan Tran. 2013. SABR goes normal. *Risk* **June** 72.

Behr, Andreas, Ulrich Pötter. 2009. Alternatives to the normal model of stock returns: Gaussian mixture, generalised logF and generalised hyperbolic models. *Annals of Finance* **5**(1) 49–68.

Biller, Bahar, Soumyadip Ghosh. 2006. Multivariate input processes. Shane G Henderson, Barry L Nelson, eds., *Handbooks in operations research and management science: Simulation*, vol. 13. Elsevier, 123–153.

Bougerol, Philippe. 1983. Exemples de théorèmes locaux sur les groupes résolubles. *Annales de l'IHP Probabilités et statistiques*, vol. 19. 369–391.

Box, George EP, Mervin E Muller. 1958. A note on the generation of random normal deviates. *The Annals of Mathematical Statistics* **29**(2) 610–611.

Brooks, Robert, Joshua A Brooks. 2017. An option valuation framework based on arithmetic Brownian motion: Justification and implementation issues. *Journal of Financial Research* **40**(3) 401–427.

Cai, Ning, Yingda Song, Nan Chen. 2017. Exact simulation of the SABR model. *Operations Research* **65**(4) 931–951.

Chen, Bin, Cornelis W Oosterlee, Hans Van Der Weide. 2012. A low-bias simulation scheme for the SABR stochastic volatility model. *International Journal of Theoretical and Applied Finance* **15**(02) 1250016.

Choi, Pilsun, Kiseok Nam. 2008. Asymmetric and leptokurtic distribution for heteroscedastic asset returns: the S_U-normal distribution. *Journal of Empirical finance* **15**(1) 41–63.

Corlu, Canan G, Alper Corlu. 2015. Modelling exchange rate returns: which flexible distribution to use? *Quantitative Finance* **15**(11) 1851–1864.

Debiard, Amédée, Bernard Gaveau, Edmond Mazet. 1976. Théoremes de comparaison en géométrie riemannienne. *Publications of the Research Institute for Mathematical Sciences* **12**(2) 391–425.

Eberlein, Ernst, Ulrich Keller, et al. 1995. Hyperbolic distributions in finance. *Bernoulli* **1**(3) 281–299.

Fama, Eugene F. 1965. The behavior of stock-market prices. *The Journal of Business* **38**(1) 34–105.

Grigor'yan, Alexander, Masakazu Noguchi. 1998. The heat kernel on hyperbolic space. *Bulletin of the London Mathematical Society* **30**(6) 643–650.

Gurrola, Pedro. 2007. Capturing fat-tail risk in exchange rate returns using S_U curves: A comparison with the normal mixture and skewed student distributions. *The Journal of Risk* **10**(2) 73.

Hagan, Patrick S, Deep Kumar, Andrew S Lesniewski, Diana E Woodward. 2002. Managing smile risk. *Wilmott* (September) 84–108.

Hagan, Patrick S, Diana E Woodward. 1999. Equivalent black volatilities. *Applied Mathematical Finance* **6**(3) 147–157.

Henry-Labordère, Pierre. 2005. A general asymptotic implied volatility for stochastic volatility models. *Available at SSRN* URL `https://ssrn.com/abstract=698601`.

Henry-Labordère, Pierre. 2008. *Analysis, geometry, and modeling in finance: Advanced methods in option pricing*. CRC Press.

Heston, Steven L. 1993. A closed-form solution for options with stochastic volatility with applications to bond and currency options. *Review of Financial Studies* **6**(2) 327–343.

Hull, John, Alan White. 1987. The pricing of options on assets with stochastic volatilities. *The Fournal of Finance* **42**(2) 281–300.

Johnson, Norman L. 1949. Systems of frequency curves generated by methods of translation. *Biometrika* **36**(1/2) 149–176.

Jones, David L. 2014. Johnson curve toolbox for Matlab: Analysis of non-normal data using the johnson family of distributions. URL `http://www.marine.usf.edu/user/djones/jctm/jctm.html`.

Jordan, Richard, Charles Tier. 2011. Asymptotic approximations to deterministic and stochastic volatility models. *SIAM Journal on Financial Mathematics* **2**(1) 935–964.

Kennedy, Joanne E, Subhankar Mitra, Duy Pham. 2012. On the approximation of the SABR model: A probabilistic approach. *Applied Mathematical Finance* **19**(6) 553–586.

Kenyon, Chris. 2008. Inflation is normal. *Risk* 54.

Kon, Stanley J. 1984. Models of stock returns: A comparison. *The Journal of Finance* **39**(1) 147–165.

Korn, Ralf, Songyin Tang. 2013. Exact analytical solution for the normal SABR model. *Wilmott* (July) 64–69.

Le Floc'h, Fabien, Gary J Kennedy. 2014. Finite difference techniques for arbitrage free SABR. *Available at SSRN* URL `https://ssrn.com/abstract=2402001`.

Leitao, Álvaro, Lech A Grzelak, Cornelis W Oosterlee. 2017a. On a one time-step Monte Carlo simulation approach of the SABR model: Application to european options. *Applied Mathematics and Computation* **293** 461–479.

Leitao, Álvaro, Lech A Grzelak, Cornelis W Oosterlee. 2017b. On an efficient multiple time step monte carlo simulation of the sabr model. *Quantitative Finance* 1–17.

Levin, Alexander. 2004. Interest rate model selection. *The Journal of Portfolio Management* **30**(2) 74–86.

Lewis, Alan L. 2000. *Option Valuation Under Stochastic Volatility*. Finance Press, Newport Beach, CA.

Lorig, Matthew, Stefano Pagliarani, Andrea Pascucci. 2015. Explicit implied volatilities for multifactor local-stochastic volatility models. *Mathematical Finance* .

Marsaglia, George, Thomas A Bray. 1964. A convenient method for generating normal variables. *SIAM Review* **6**(3) 260–264.

Matsumoto, Hiroyuki, Marc Yor. 2005a. Exponential functionals of Brownian motion, I: Probability laws at fixed time. *Probability Surveys* **2** 312–347.

Matsumoto, Hiroyuki, Marc Yor. 2005b. Exponential functionals of Brownian motion, II: Some related diffusion processes. *Probability Surveys* **2** 348–384.

McKean, Henry P, et al. 1970. An upper bound to the spectrum of Δ on a manifold of negative curvature. *Journal of Differential Geometry* **4**(3) 359–366.

Mills, Terence C. 1995. Modelling skewness and kurtosis in the London stock exchange FT-SE index return distributions. *The Statistician* 323–332.

Obłój, Jan. 2007. Fine-tune your smile: Correction to Hagan et al. *Available at arXiv* URL `https://arxiv.org/pdf/0708.0998`.

Park, Hyukjae. 2014. SABR symmetry. *Risk* **January** 106–111.

Poitras, Geoffrey. 1998. Spread options, exchange options, and arithmetic Brownian motion. *Journal of Futures Markets* **18**(5) 487–517.

Schachermayer, Walter, Josef Teichmann. 2008. How close are the option pricing formulas of Bachelier and Black–Merton–Scholes? *Mathematical Finance* **18**(1) 155–170.

Shang, Jen S, Pandu R Tadikamalla. 2004. Modeling financial series distributions: A versatile data fitting approach. *International Journal of Theoretical and Applied Finance* **7**(03) 231–251.

Simonato, Jean-Guy. 2011. The performance of Johnson distributions for computing value at risk and expected shortfall. *The Journal of Derivatives* **19**(1) 7–24.

Stein, Elias M, Jeremy C Stein. 1991. Stock price distributions with stochastic volatility: an analytic approach. *The Review of Financial Studies* **4**(4) 727–752.

Theodossiou, Panayiotis. 1998. Financial data and the skewed generalized t distribution. *Management Science* **44**(12-part-1) 1650–1661.

Tuenter, Hans JH. 2001. An algorithm to determine the parameters of S_U-curves in the Johnson system of probabillity distributions by moment matching. *Journal of Statistical Computation and Simulation* **70**(4) 325–347.

Vakeroudis, Stavros. 2012. Bougerol's identity in law and extensions. *Probability Surveys* **9** 411–437.

Venkataraman, Sree Vinutha, SVD Nageswara Rao. 2016. Estimation of dynamic VaR using JSU and PIV distributions. *Risk Management* **18**(2-3) 111–134.

Wheeler, Robert E. 1980. Quantile estimators of johnson curve parameters. *Biometrika* 725–728.

Wu, Qi. 2012. Series expansion of the SABR joint density. *Mathematical Finance* **22**(2) 310–345.

Yor, Marc, ed. 1997. *Exponential Functionals and Principal Values related to Brownian Motion. A collection of research papers*. Biblioteca de la Revista Matematicá Iberoamericana.

Yor, Marc. 2012. *Exponential functionals of Brownian motion and related processes*. Springer Science & Business Media.